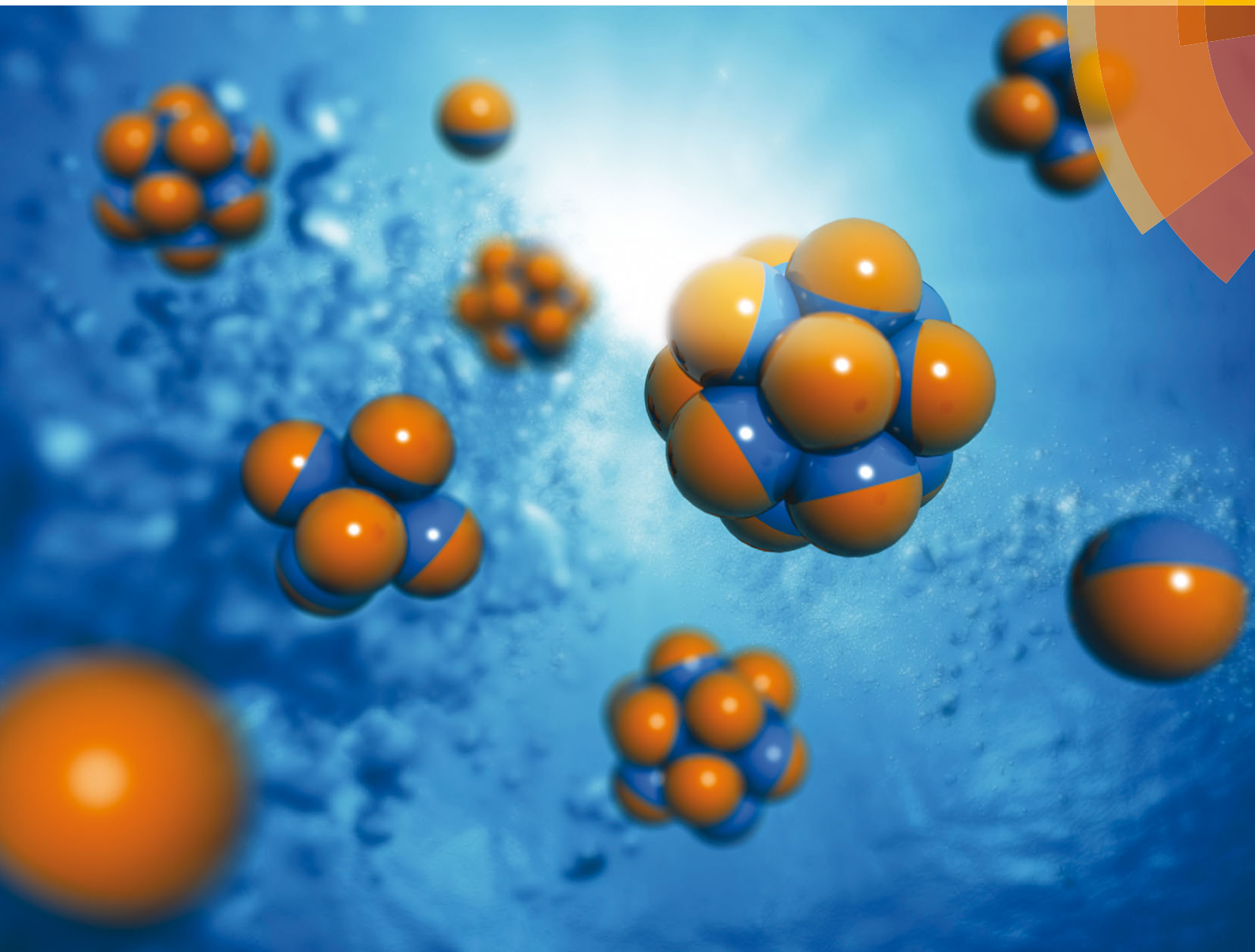


Soft Matter

www.softmatter.org



ISSN 1744-683X



COMMUNICATION

Arash Nikoubashman *et al.*

Self-assembly of Janus particles under shear



Self-assembly of Janus particles under shear

Emanuela Bianchi,^a Athanassios Z. Panagiotopoulos^b and Arash Nikoubashman^{*b}

Cite this: *Soft Matter*, 2015, **11**, 3767

Received 3rd February 2015,
Accepted 15th March 2015

DOI: 10.1039/c5sm00281h

www.rsc.org/softmatter

We investigate the self-assembly of colloidal Janus particles under shear flow by employing hybrid molecular dynamics simulations that explicitly take into account hydrodynamic interactions. Under quiescent conditions, the amphiphilic colloids form spherical micellar aggregates of different sizes, where the solvophobic hemispheres are directed towards the core and the solvophilic caps are exposed to the solvent. When sufficiently strong shear is applied, the micelles disaggregate with a consequent decay of the average cluster size. Nonetheless, we find an intermediate shear rate regime where the balance between rearrangement and dissociation favors the growth of the aggregates. Additionally, our simulations show that clusters composed of either 6 or 13 particles are the most stable towards the shear flow due to their high geometric symmetry. Our findings open up a new range of applications for Janus particles, ranging from biotechnology to sensor systems.

Janus particles, named after the double-faced Roman god, have two distinguishable hemispheres, characterized by different surface properties;¹ these particles represent the simplest realization of patchy colloids.^{2,3} Fabrication methods yielding large quantities of Janus particles and guaranteeing a precise control over the properties of the two hemispheres have significantly progressed, providing either organic, inorganic or polymer based two-faced units.⁴ The interest in such entities lies in a broad range of applications for which they are suitable, *e.g.*, as self-propelling sensors,⁵ micro-rheological probes,⁶ and biomedical nano devices for drug delivery and cell targeting.⁷ Experimental and numerical investigations of Janus particles in the bulk have highlighted a rich assembly scenario: according to the characteristics of specific systems, Janus particles can form well-defined aggregates, such as micelles, vesicles, or lamellar phases.^{8,9} In particular, it has been shown that, at low solute concentrations and sufficiently low temperatures (or high interaction strengths), amphiphilic Janus

particles form micellar aggregates, where the solvophobic parts of the particles are directed towards the aggregate center to minimize contact with the solvent. At first glance, this self-assembly scenario bears a strong resemblance to flexible amphiphiles. However, in contrast to these conventional surfactant molecules, Janus particles are rigid and carry both the solvophilic and solvophobic part on the *same* bead.

In the present paper, we investigate the effect of shear flow on the self-assembly behavior of Janus particles. In general, the effect of shear on particle aggregation can be very diverse. It can enhance growth, breakup, or coalescence of colloidal aggregates,¹⁰ trigger a transition from a crystal to a uniform phase,¹¹ or induce the formation of ordered non-equilibrium structures, such as lattices or sliding particle planes.^{12–14} We focus on the micellar phase of Janus systems and find that they respond to shear in a novel way, which markedly differs from previously investigated clustering systems:^{13,15} small shear enhances the aggregation into spherical clusters, before they are finally broken up as the shear rate is increased further. Here, it is peculiar that the shear-induced breakup is enhanced with increasing solute density, which is in stark contrast to systems of isotropically interacting cluster formers.^{15–17} In addition, our simulations show that aggregates composed of either 6 or 13 particles are the most stable due to their high symmetry.

In our simulations, we model the interaction between two Janus particles of diameter σ *via*:⁹

$$U(\mathbf{r}_{ij}, \mathbf{q}_i, \mathbf{q}_j) = U_{\text{WCA}}(r_{ij}) + U_{\text{Janus}}(\mathbf{r}_{ij}, \mathbf{q}_i, \mathbf{q}_j), \quad (1)$$

where $\mathbf{r}_{ij} = \mathbf{r}_j - \mathbf{r}_i$ denotes the inter-particle distance and $\mathbf{q}_{i,j}$ represents the director of particle i, j . The potential is composed of two terms: U_{WCA} is the standard purely repulsive WCA potential,¹⁸ while U_{Janus} is the anisotropic contribution due to the patchiness of the colloids. The functional form of U_{Janus} is given by:¹⁹

$$U_{\text{Janus}}(\mathbf{r}_{ij}, \mathbf{q}_i, \mathbf{q}_j) = \frac{C \exp[-\lambda(r_{ij} - \sigma)]}{r_{ij}^2} (\mathbf{q}_i - \mathbf{q}_j) \cdot \mathbf{r}_{ij}, \quad (2)$$

where the parameters C and λ set the interaction strength and length, respectively. We set $\lambda = 3\sigma^{-1}$ to avoid the unphysical

^a Institute of Theoretical Physics, Vienna University of Technology, Wiedner Hauptstraße 8-10, A-1040 Vienna, Austria

^b Department of Chemical and Biological Engineering, Princeton University, Princeton, New Jersey 08544, USA. E-mail: arashn@princeton.edu

formation of tetralayers,¹⁹ and consider C values in the range of $5-7k_B T$.

The simulations were conducted in a slit-like channel with volume $V = L_x \times L_y \times L_z$ with periodic boundary conditions in the vorticity and flow directions (y and z). The two impenetrable walls, placed perpendicular to the gradient direction at $x = 0$ and $x = L_x$, have been modeled by a soft repulsive potential.²⁰ We employed the standard velocity Verlet algorithm for computing the translational motion of the solute particles, and used a quaternion-based algorithm to resolve the rigid-body dynamics.²¹

Hydrodynamic interactions were incorporated using the Multi Particle Collision Dynamics (MPCD) simulation scheme,²² where the surrounding Newtonian solvent is modeled as $\rho_s V$ ideal point particles with unit mass $m = 1$. The motion of the solvent particles is governed by alternating streaming and collision steps: first, all solvent particles propagate ballistically over a period of Δt_{MPCD} . Then they are sorted into cubic cells with edge length a , and undergo a stochastic collision with particles in the same cell. In our implementation of the algorithm, this process is mimicked through a collective rotation of the solvent velocities around a randomly chosen unit vector with a fixed angle α . The Janus particles are coupled to the solvent through momentum transfer during the streaming step, following the algorithm described in ref. 20. Due to the cell-based nature of this algorithm, Galilean invariance is violated for mean-free paths $\xi = \sqrt{k_B T / m \Delta t_{\text{MPCD}}} < a/2$; therefore, we performed random lattice shifts before each collision step.²³ Furthermore, the spatial resolution of the hydrodynamic interactions is determined by the mesh size of the collision cells, and we set $\sigma = 3a$ to correctly resolve the fluid flow around the individual colloids.²⁰

Shear flow with shear rate $\dot{\gamma} = 2v_s/L_x$ was incorporated into the system by rescaling the average solvent velocity in the MPCD cells adjacent to the shear plane in such a way that it matched the wall velocity $\pm v_s$.^{13,24} Like in any non-equilibrium simulation, thermostatting is required for maintaining isothermal conditions and preventing viscous heating effects. We achieved this by rescaling the solvent velocities on the cell level. The solute particles were then thermalized through collisions with the solvent particles, leading to the correct Maxwell-Boltzmann distribution of their translational and rotational velocities in equilibrium. We used $L_x = 10\sigma$ and $L_y = L_z = 20\sigma$, a solvent density of $\rho_s a^3 = 5$, a collision angle of $\alpha = 130^\circ$, and a timestep of $\Delta t_{\text{MD}} = 0.002$ and $\Delta t_{\text{MPCD}} = 0.1$ for the molecular dynamics (MD) and MPCD step, respectively. All simulations have been conducted at $T = 1$. In what follows, we will use σ and $k_B T$ as our unit of length and energy, respectively, while we express the unit of time by the intrinsic time scale of the MPCD algorithm $\tau = \sqrt{ma^2/k_B T}$. In our simulations, we increased $\dot{\gamma}\tau$ from 0.00 to 0.08 in steps of 0.005. Using the Stokes-Einstein equation $D = k_B T / (3\pi\eta\sigma)$, we can establish a relation to experiments. For an aqueous solvent (e.g. hexane) at room temperature and solute diameters of $\sigma = 50-100$ nm, we can conclude that the applied shear rates are on the order of 10 s^{-1} to 10^3 s^{-1} , which is in the experimentally accessible regime.

First, we focused on the shear response of single Janus micelles for various aggregation numbers M . In particular, we determined the critical shear rate $\dot{\gamma}_{\text{crit}}$ required for breaking a

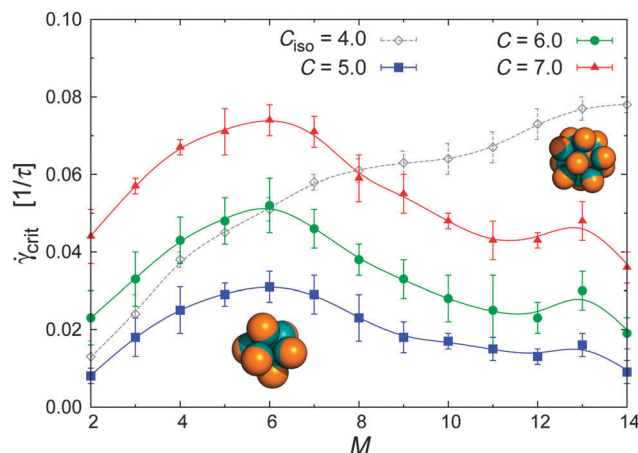


Fig. 1 Critical shear rate $\dot{\gamma}_{\text{crit}}$ required to break up a single cluster consisting of M particles for three C values and for the isotropic case (as labeled). Janus particles are represented by two hemispheres, the turquoise one features the solvophobic (attractive) part, while the orange one represents the solvophilic (repulsive) part.

cluster up, *i.e.* detaching a particle from the cluster. Two Janus particles were assigned to the same cluster, when $|\mathbf{r}_i - \frac{1}{2}\sigma\mathbf{q}_i - \mathbf{r}_j + \frac{1}{2}\sigma\mathbf{q}_j| < \sigma$, *i.e.* the distance between the poles of their solvophobic hemispheres were within one particle diameter. Furthermore, the cluster was considered stable when its composition remained unchanged over 10^4 MD steps. This additional constraint ensures that particles, which are brought close to a given cluster by the flow, are not erroneously considered as part of the cluster.

For each state point, we ran 10 independent simulations of a single cluster of size M (each lasting 5×10^6 timesteps). Fig. 1 shows $\dot{\gamma}_{\text{crit}}$ as a function of M for three values of the interaction strength C . Besides the expected increase of $\dot{\gamma}_{\text{crit}}$ with C , a peculiar non-monotonic behavior is revealed by the presence of two local maxima, one (higher) at $M = 6$ and the other (lower) at $M = 13$. These maxima are due to the high structural symmetry of the spontaneously formed aggregates at $M = 6$ (octahedron) and $M = 13$ (icosahedron), as shown by the simulation snapshots in Fig. 1. These aggregates are nearly spherical and are isotropically delimited by solvophilic hemispheres. In contrast, clusters with $M \neq 6, 13$ exhibit a considerably lower symmetry and have exposed solvophobic patches that can lead to further bonding.

To better understand the enhanced stability of clusters with $M = 6$ (and $M = 13$ to a lower extent), we measured the potential energy per particle $E(0)/M$ and the radius of gyration $R_g(0)$ of aggregates with different M values at zero shear. Fig. 2(a) shows that $E(0)/M$ quickly decays with increasing aggregation number until it remains approximately constant for $M > 6$. This smaller linear decrease of $E(0)$ for $M > 6$ is due to the breakup of the translational and rotational symmetry of the octahedral $M = 6$ cluster, which is inevitable for accommodating additional particles in the cluster. At the same time, however, $R_g(0)$ keeps increasing monotonically as shown in Fig. 2(b). The size of the micelle increases as more particles are added to the cluster, thereby exposing the aggregate to stronger shear forces. The local maximum

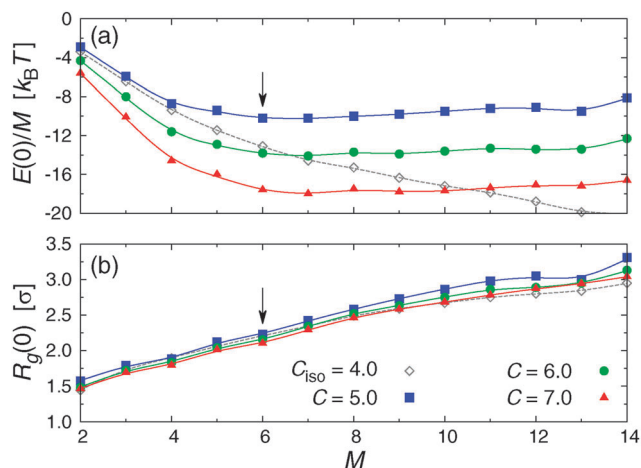


Fig. 2 (a) Energy per particle $E(0)/M$ and (b) radius of gyration $R_g(0)$ at zero shear rate for clusters consisting of M particles for three C values and for the isotropic case (as labeled). Measurement uncertainty is $<2\%$ for both $E(0)/M$ and $R_g(0)$, leading to error bars smaller than the symbol size. Arrows indicate the position of the global maximum of $\dot{\gamma}_{\text{crit}}$.

at $M = 13$ in Fig. 1 is well above the measurement uncertainty and is due to the mechanical stability of the icosahedral cluster morphology. This configuration maximizes the number of nearest-neighbor bondings,⁹ while keeping the cluster relatively compact.

In order to investigate the effect of interaction anisotropy in more detail, we conducted additional simulations in the limiting isotropic case of purely solvophobic particles. This was achieved by fixing $(\mathbf{q}_i - \mathbf{q}_j) \cdot \mathbf{r}_{ij}/r_{ij} = -2$ in eqn (2). The results for isotropic interactions with $C_{\text{iso}}=4$ are included in Fig. 1 and 2. It is evident that the shear response markedly differs from the Janus case: (i) $\dot{\gamma}_{\text{crit}}$ increases monotonically with the aggregate size, (ii) $\dot{\gamma}_{\text{crit}}$ is always higher for the isotropic case although $C_{\text{iso}} < C$, and (iii) $E(0)/M$ does not reach a plateau as it does for the Janus particles.

These differences help us to understand the mechanism behind the shear-induced cluster breakup. The imposed shear causes a net force, which pulls the aggregated colloids apart from each other. In addition, as the solvent flows past the aggregate, it applies a torque on both the whole aggregate and the individual colloids, causing them to rotate. For isotropic particles, the rotation of the individual particles does not have any impact on the bonding energies, and therefore is negligible. In the case of the Janus particles, however, the rotation of the constituent particles can lead to the weakening of the inter-particle attractions, which in turn reduces the $\dot{\gamma}_{\text{crit}}$ needed to break one particle bond. To better understand this process, we have schematically drawn it in Fig. 3.

Next, we studied the shear behavior of Janus particles with $C = 6.0$ at number densities $\rho = 0.05, 0.10, 0.15,$ and 0.20 . Under quiescent conditions, we found a rather broad cluster distribution, where the average cluster size $\langle M \rangle$ increased with increasing ρ . Fig. 4 shows the average cluster size $\langle M \rangle$ as a function of the applied shear rate $\dot{\gamma}$, and we can immediately discern a remarkable feature: the formation of micelles is enhanced at sufficiently small $\dot{\gamma}$,

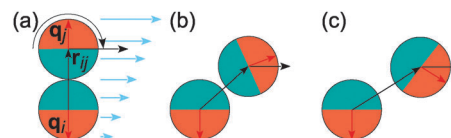


Fig. 3 Schematic representation of the shear-induced breakup of a Janus dumbbell in the reference frame of particle i . (a) Initially, the solvophobic hemispheres of both colloids are facing each other, resulting in maximum attraction. (b) Then, shear leads to a displacement and rotation of particle j , decreasing the mutual attraction. (c) Finally, the attractive contribution in U_{Janus} becomes sufficiently small so that shear can break the pair up.

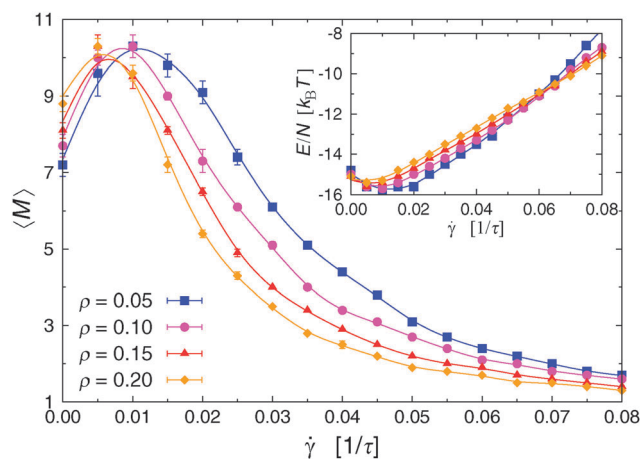


Fig. 4 Main: average cluster size $\langle M \rangle$ vs. shear rate $\dot{\gamma}$ for different ρ -values (as labeled). Inset: energy per particle E/N vs. shear rate $\dot{\gamma}$.

which is reflected in the initial increase of $\langle M \rangle$. In the low $\dot{\gamma}$ regime, shear can help to breakup and reform aggregates which have energetically unfavorable configurations. Furthermore, shear flow increases the mobility of the dispersed particles, which in turn improves the probability of merging free particles and underpopulated aggregates. However, this process cannot be sustained indefinitely, and $\langle M \rangle$ rapidly decays when $\dot{\gamma}$ is increased further.

Another peculiarity of the system is that $\langle M \rangle$ decreases with increasing ρ when sufficient shear is applied to the system. At the same time, the maximum of $\langle M \rangle$ shifts to lower $\dot{\gamma}$. The reason for these trends is that the clusters collide more frequently with each other at high particle densities, resulting in an increased disassociation of particles. This collective behavior is unique to these amphiphilic micelles, and stems from the short-ranged repulsion of the solvophilic shells. The evolution from shear-induced cluster growth to eventual cluster breakup is also reflected in the energy per particle E/N reported in the inset of Fig. 4, confirming the validity of our clustering criterion.

Additionally, we measured the probability to find a particle in a cluster of a size M , $p(M)$, for various shear rates and report the resulting data for $\rho = 0.10$ in Fig. 5. At zero shear, the cluster sizes range between $M = 4$ and 15 with a maximum at $M = 8$. When the shear is turned on ($\dot{\gamma} = 0.01$), most of the particles can be found in icosahedral micelles of size $M = 13$. On further

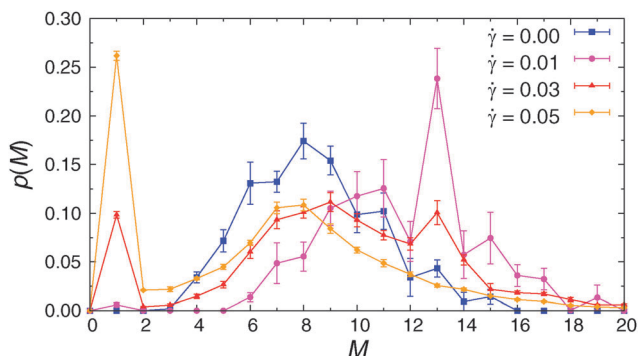


Fig. 5 Probability of a particle to be in a cluster of size M , $p(M)$, for various shear rates (as labeled) at $\rho = 0.10$.

increasing the shear rate ($\dot{\gamma} = 0.03$), clusters start breaking up, which is reflected by the shift of $p(M)$ to lower M values and by the emerging peak at $M = 1$. This trend continues with increasing shear, and at $\dot{\gamma} = 0.05$ we found that the number of free monomers exceeds the number of clustered particles. Finally, it is worth noting that shear promotes the formation of (few) rather large aggregates even at rather high $\dot{\gamma}$. For instance, the maximum aggregation number at rest was $M = 15$, while we found clusters with up to $M = 25$ particles at $\dot{\gamma} = 0.05$.

In order to highlight the peculiar shear response of the Janus particles due to their anisotropy, we conducted additional simulations of isotropically interacting systems. However, special care has to be taken at *finite* densities, since purely attractive particles will collapse into a single large aggregate corresponding to a first-order phase transition at a temperature-dependent density. To impede such unbounded cluster growth for isotropic particles, we complemented the short range attraction (SA), required for the cluster formation, with a long range repulsion (LR) to stabilize the clusters.^{15–17} The functional form of the pair potential is then given by:

$$U_{\text{SALR}} = 4\epsilon \left[\left(\frac{\sigma}{r_{ij}} \right)^{2\alpha} - \left(\frac{\sigma}{r_{ij}} \right)^\alpha \right] + D \frac{e^{-r_{ij}/\xi}}{r_{ij}/\xi}. \quad (3)$$

To make meaningful comparisons to the Janus systems, the parameters in eqn (3) need to be carefully tuned to match $\langle M \rangle$ and E/N at all investigated densities. This is however a difficult undertaking, since the isotropic systems exhibit a strong tendency to form large anisotropic clusters upon increasing the density ρ .^{15–17} For $\alpha = 20$, $\epsilon = 10k_{\text{B}}T$, $D = 2k_{\text{B}}T$ and $\xi = 2\sigma$, we observed the spontaneous formation of spherical micelles at $\rho = 0.05$ and 0.10 , whereas we found a sizable number of anisotropic aggregates at higher densities. Therefore, we will concentrate on the lower density cases.

The first remarkable difference with respect to Janus particle aggregates is that at zero shear, the system forms a crystalline structure, where each lattice is occupied by a colloidal cluster. This effect is due to the slowly-decaying repulsive tail in U_{SALR} , which induces long range order. At low shear rates, the layers move against each other, while keeping the in-plane order intact. Upon increasing $\dot{\gamma}$, clusters from neighboring layers are pushed

towards each other and start to merge. As the shear is increased even further, shear forces eventually break up the clusters into smaller pieces. However, in contrast to the Janus particles, the average cluster size $\langle M \rangle$ increases with increasing particle density ρ , since colliding aggregates can merge. A similar behavior has been also observed recently for two-dimensional cluster crystals interacting *via* interactions of the same family.¹⁵ Furthermore, we were unable to identify any characteristic aggregation numbers contrary to the Janus case.

In summary, we have investigated the behavior of Janus colloids under shear in the temperature and concentration regime that favors micelle formation. We found that shear flow can enhance the formation of colloidal micelles and induce the aggregation of bigger clusters. Moreover, we have highlighted the micelle morphologies that are more resistant to the dissociation induced by the shear flow and we have shown that a small shear rate can push the system to form mainly icosahedral micelles that can be disassembled on further increasing the shear flow. We surmise that hydrodynamic effects play an important role for both the self-assembly and the dynamics of these clustering systems. This is especially true for rather large clusters, where some of the colloids are completely shielded from the surrounding solvent. In addition, solvent depletion effects might also play an important role for the cluster stability, and merit further investigation.

The shear-induced breakup of Janus micelles can be relevant for biomedical applications when the solvophobic shell is coated with a drug.²⁵ Another potential application of the observations in this work can be in the development of shear-rate sensors, by utilizing clusters with optical properties sensitive to the cluster aggregation number. The simulations presented in this work might also shed some light on the extrusion process by which self-assembled structures of amphiphilic moieties in nanoporous materials are broken up into smaller structures by shear;²⁶ this process is heavily used both in biomedical research and industrial processes for dairy products and cosmetics.

Acknowledgements

A.N. and A.Z.P. acknowledge financial support from the Princeton Center for Complex Materials (PCCM), a U.S. National Science Foundation Materials Research Science and Engineering Center (Grants DMR-0819860 and DMR-1420541). E.B. acknowledges financial support by the Austrian Science Foundation (FWF) under project number V249-N27. This work used the Extreme Science and Engineering Discovery Environment (XSEDE), which is supported by National Science Foundation grant number ACI-1053575.

References

- 1 A. Walther and A. H. E. Müller, *Chem. Rev.*, 2013, **113**, 5194.
- 2 A. B. Pawar and I. Kretzschmar, *Macromol. Rapid Commun.*, 2010, **31**, 150.
- 3 E. Bianchi, R. Blaak and C. N. Likos, *Phys. Chem. Chem. Phys.*, 2011, **13**, 6397.
- 4 C. Kaewsaneha, P. Tangboriboonrat, D. Polpanich, M. Eissa and A. Elaissari, *ACS Appl. Mater. Interfaces*, 2013, **5**, 1857.

- 5 A. Brown and W. Poon, *Soft Matter*, 2014, **10**, 4016.
- 6 C. J. Behrend, J. N. Anker, B. H. McNaughton, M. Brasuel, M. A. Philbert and R. Kopelman, *J. Phys. Chem. B*, 2004, **108**, 10408.
- 7 S. Yang, F. Guo, B. Kiraly, X. Mao, M. Lu, K. W. Leong and T. J. Huang, *Lab Chip*, 2012, **12**, 2097.
- 8 F. Sciortino, A. Giacometti and G. Pastore, *Phys. Rev. Lett.*, 2009, **103**, 237801.
- 9 G. Rosenthal, K. E. Gubbins and S. H. L. Klapp, *J. Chem. Phys.*, 2012, **136**, 174901.
- 10 R. J. Allen, C. Valeriani, S. Tănase-Nicola, P. R. ten Wolde and D. Frenkel, *J. Chem. Phys.*, 2008, **129**, 134704.
- 11 R. Seto, R. Botet, G. K. Auernhammer and H. Briesen, *Eur. Phys. J. E: Soft Matter Biol. Phys.*, 2012, **35**, 128.
- 12 Y. L. Wu, D. Derks, A. van Blaaderen and A. Imhof, *Proc. Natl. Acad. Sci. U. S. A.*, 2009, **106**, 10564.
- 13 A. Nikoubashman, G. Kahl and C. N. Likos, *Phys. Rev. Lett.*, 2011, **107**, 068302.
- 14 B. Lander, U. Seifert and T. Speck, *J. Chem. Phys.*, 2013, **138**, 224907.
- 15 A. Imperio, L. Reatto and S. Zapperi, *Phys. Rev. E: Stat., Nonlinear, Soft Matter Phys.*, 2008, **78**, 021402.
- 16 F. Sciortino, S. Mossa, E. Zaccarelli and P. Tartaglia, *Phys. Rev. Lett.*, 2004, **93**, 055701.
- 17 S. Mossa, F. Sciortino, P. Tartaglia and E. Zaccarelli, *Langmuir*, 2004, **20**, 10756.
- 18 J. D. Weeks, D. Chandler and H. C. Andersen, *J. Chem. Phys.*, 1971, **54**, 5237.
- 19 A. M. Somoza, E. Chacón, L. Mederos and P. Tarazona, *J. Phys.: Condens. Matter*, 1995, **7**, 5753.
- 20 A. Nikoubashman, C. N. Likos and G. Kahl, *Soft Matter*, 2013, **9**, 2603.
- 21 D. Rozmanov and P. G. Kusalik, *Phys. Rev. E: Stat., Nonlinear, Soft Matter Phys.*, 2010, **81**, 056706.
- 22 A. Malevanets and R. Kapral, *J. Chem. Phys.*, 1999, **110**, 8605.
- 23 T. Ihle and D. M. Kroll, *Phys. Rev. E: Stat., Nonlinear, Soft Matter Phys.*, 2001, **63**, 020201.
- 24 M. Hecht, J. Harting, M. Bier, J. Reinshagen and H. J. Herrmann, *Phys. Rev. E: Stat., Nonlinear, Soft Matter Phys.*, 2006, **74**, 021403.
- 25 Y. Gao and Y. Yu, *J. Am. Chem. Soc.*, 2013, **135**, 19091.
- 26 L. Mayer, M. Hope and P. Cullis, *Biochim. Biophys. Acta*, 1986, **858**, 161.